Anisotropic Modification of the Effective Hole g Factor by Electrostatic Confinement

S. P. Koduvayur,[1,*] L. P. Rokhinson,[1] D. C. Tsui,[2] L. N. Pfeiffer,[3] and K. W. West[3]

[1]*Department of Physics, Purdue University, West Lafayette, Indiana 47907 USA*
[2]*Department of Electrical Engineering, Princeton University, Princeton, New Jersey 08544 USA*
[3]*Bell Laboratories, Lucent Technologies, Murray Hill, New Jersey 07974 USA*

(Received 18 July 2007; published 28 March 2008)

We investigate effects of lateral confinement on spin splitting of energy levels in 2D hole gases grown on [311] GaAs. We found that lateral confinement enhances anisotropy of spin splitting relative to the 2D gas for both confining directions. Unexpectedly, the effective g factor does not depend on the 1D energy level number N for $B \parallel [0\bar{1}1]$ while it has strong N dependence for $B \parallel [\bar{2}33]$. Apart from quantitative difference in the spin splitting of energy levels for the two orthogonal confinement directions, we also report qualitative differences in the appearance of spin-split plateaus, with nonquantized plateaus observed only for the confinement in the $[0\bar{1}1]$ direction. In our samples we can clearly associate the difference with anisotropy of spin-orbit interactions.

DOI: 10.1103/PhysRevLett.100.126401 PACS numbers: 71.70.Ej, 71.18.+y, 73.23.Ad

Devices that use spin as the main carrier of information promise higher speeds and lesser energy demands and have been the bases for the new fields of spintronics and quantum information [1,2]. An important aspect in the realization of these devices is efficient manipulation and control of spins. GaAs hole systems provide a potential advantage in electrostatic manipulation of spins due to stronger spin-orbit (SO) interaction, compared to electronic systems. With predictions of increasing spin-relaxation times in p-type based low-dimensional systems [3] to orders comparable to those of electrons, there is a need to better understand the physics of SO interactions.

In two-dimensional GaAs hole gases (2DHG) grown in the [001] crystallographic direction, SO locks spins in the growth direction resulting in a vanishing spin response to the in-plane magnetic field (vanishing effective Landé g factor g^*) [4,5]. For high-index growth directions, such as [311], in-plane g^* is not zero and becomes highly anisotropic [6]. Additional lateral confinement increases g^* anisotropy [7], and the value depends on the population of 1D subbands [8]. Strong suppression of g^* for the in-plane magnetic field perpendicular to the channel direction has been attributed to the confinement-induced reorientation of spins perpendicular to the 1D channel [8]. In this Letter we demonstrate that the anisotropy of spin splitting is primarily due to the crystalline anisotropy of SO interactions and not the lateral confinement. We investigate quantum point contacts with confinement in both $[0\bar{1}1]$ and $[\bar{2}33]$ directions and find that anisotropy of spin splitting depends on the field direction rather than on the direction of the lateral confinement. There is a strong dependence of g^* on the number of filled 1D subbands N for one field direction ($B \parallel [\bar{2}33]$), while g^* is almost N independent for the orthogonal field direction ($B \parallel [0\bar{1}1]$). We also report qualitative differences in the appearances of the conductance plateaus for the two orthogonal confinement directions. For the channels confined in the $[\bar{2}33]$ direction the conductance of spin-split plateaus is $(N + 1/2) \times 2e^2/h$, in accordance with the Landauer formula. For the orthogonal direction nonquantized plateaus appear that have some resemblance to the so-called "0.7 structure" [9] (an extra plateau at $0.7 \times 2e^2/h$) and its various "analogs" [10], and their conductance values change with magnetic field. The major difference between the two orientations of 1D channels in our experiments is the strength of SO, which may provide some clues to the origin of these yet-to-be-understood anomalies.

We use atomic force microscope (AFM) local anodic oxidation [11] to fabricate the quantum point contacts (QPCs), which results in a sharper potential compared to the top gating technique and also eliminates leakage problems associated with low Schottky barriers in p-type GaAs. The use of this technique requires specially designed heterostructures with very shallow 2DHG, details of which are given in [12]. An AFM image of a QPC device is shown in the inset in Fig. 1. White lines are oxide, which separates 2DHG into source (S), drain (D), and gate (G) regions; the 2DHG is depleted underneath the oxide. The side gates are used to electrostatically control the width of the 1D channel. AFM lithography aids in precise control of QPC dimensions with corresponding pinch-off voltage control within a few mV, allowing comparison of orthogonal QPCs with similar confining potential. At $T = 4$ K, QPCs show regular smooth field-effect transistor characteristics as a function of gate voltage. For orthogonal QPCs with similar pinch-off voltages, resistances differ by a factor of 2, reflecting the underlying anisotropy of the 2DHG. Conductivity of 2DHG on [311] GaAs is anisotropic due to a combination of the effective mass anisotropy and difference in surface morphology, with $[\bar{2}33]$ being high-mobility and $[0\bar{1}1]$ low-mobility directions [13].

Typical conductance of QPCs at low temperatures is shown in Figs. 1 and 2. Leftmost curves are measured for $B = 0$. Four-terminal resistance is corrected for the gate-independent series resistance of the adjacent 2D gas, $R_0 = 300$–$600\ \Omega$ in different samples. R_0 was also cor-

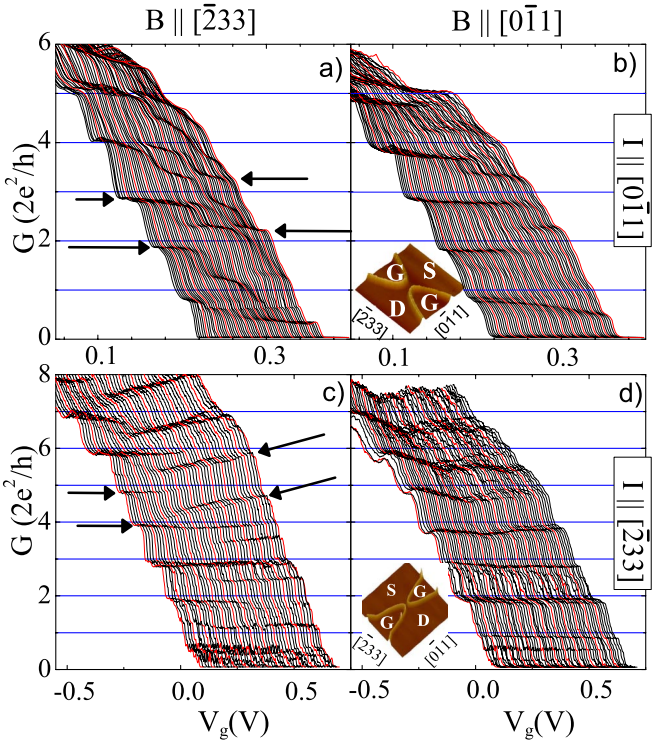

FIG. 1 (color online). Conductance of QPCs as a function of gate voltage. The curves are offset proportional to B with 0.25 T interval. Leftmost curve corresponds to $B = 0$. (a),(b) are for the channel along [0$\bar{1}$1] and (c),(d) for the channel along [$\bar{2}$33]. The arrows highlight a few plateaus discussed in the text, the slope of the arrows highlighting the slope of the corresponding plateau. Insets: 2 μm $\times$ 2 μm AFM micrographs of devices.

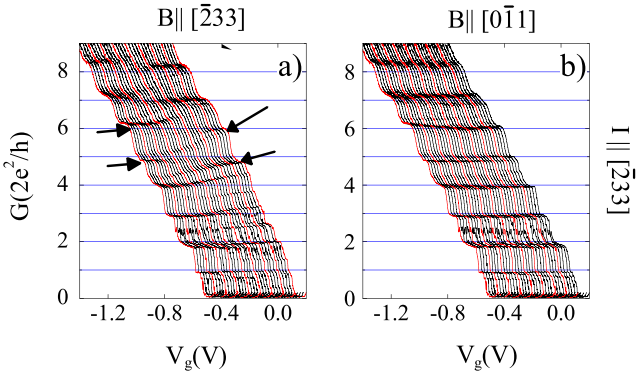

FIG. 2 (color online). Conductance of another QPC with the channel oriented along [$\bar{2}$33]. The curves are offset proportional to B with 0.25 T interval. Leftmost curve corresponds to $B = 0$. The arrows highlight plateaus discussed in the text.

rected for its B dependence, which was measured separately for both crystallographic directions (a 20% increase at 12 T). For the sample studied in Figs. 1(a) and 1(b) the 1D channel is confined in the [$\bar{2}$33] direction ($I \parallel [0\bar{1}1]$), while in Figs. 1(c), 1(d), 2(a), and 2(b) it is confined in the [0$\bar{1}$1] direction ($I \parallel [\bar{2}33]$). At low temperatures conductance is quantized [14–16] in units of $G = Ng_0$, where $g_0 = 2e^2/h$ and N is the number of 1D channels below the Fermi energy, which reflects the exact cancellation of the carriers' velocity and the density of states in 1D conductors. The factor 2 reflects spin degeneracy of energy levels at $B = 0$. Plateaus appear when electrochemical potentials of source and drain lie in the gap between neighboring 1D subbands E^N and E^{N+1}. In various samples we resolve up to 10 plateaus at temperatures $T < 100$ mK.

The effect of the in-plane magnetic field on conductance is shown in Figs. 1 and 2 for the two orthogonal field directions. The curves are offset proportional to the magnetic field with 0.25 T increments. The samples were rotated either *in situ* (Fig. 2) or after thermocycling to room temperature (Fig. 1). Mesoscopic changes during thermocycling are reflected in a small difference between the $B = 0$ curves, yet they do not change level broadening and the onset of spin splitting significantly.

There are both quantitative and qualitative differences in the field response of orthogonally oriented 1D channels. We begin the analysis with a quantitative comparison of spin splitting of energy levels for different orientations of magnetic field and channel directions. In general, the energy spectrum for holes contains linear, cubic, and higher-order terms in B [17]. At low fields the linear term dominates, and we approximate spin splitting by the Zeeman term with an effective g factor, $E_Z = 2g^*_{[ijk],N}\mu_B B$, where μ_B is the Bohr magneton and $g^*_{[ijk],N}$ depends on field orientation $B \parallel [ijk]$, energy level number N, and confine-

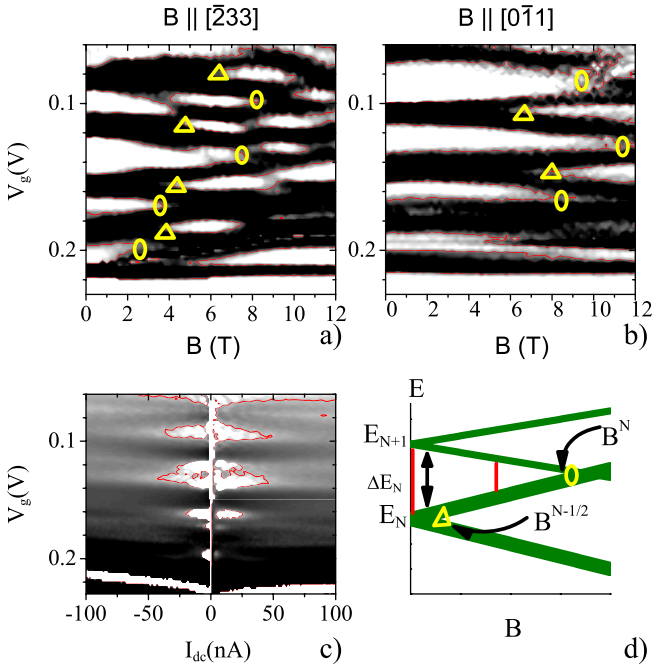

FIG. 3 (color online). (a),(b) Derivative of curves in Figs. 1(a) and 1(b), white regions correspond to the conductance plateaus. (c) Differential transresistance plotted in a logarithmic scale [from 0.01 kΩ (white) to 0.2 kΩ (black)] for the same sample at $B = 0$. (d) Schematic of Zeeman splitting of energy levels.

TABLE I. (a) Experimental values used to extract g^* for different energy levels for channel along $[0\bar{1}1]$ and (b) along $[\bar{2}33]$.

(a) N	R (kΩ)	$I_{\max}$ (nA)	ΔE_N (μeV)	$B^N_{[\bar{2}33]}$ (T)	$\langle g^*_{[\bar{2}33],N}\rangle$	$B^N_{[0\bar{1}1]}$ (T)	$\langle g^*_{[0\bar{1}1],N}\rangle$	$g^*_{[\bar{2}33]}/g^*_{[0\bar{1}1]}$	$g^*_{[\bar{2}33]}$
1	12.9	6	80			4.5	0.31		
2	6.45	23	150	3.6	0.73	8	0.32	3	0.94
3	4.3	40	170	7.5	0.4	10	0.30	2	0.6
4	3.225	50	160	8	0.34	9	0.31	1.8	0.56
5	2.58	60	150	7.3	0.36	9	0.29	1.2	0.35

(b) N	R (kΩ)	$I^{B=0}_{\max}$(nA)	$\Delta E^{B=0}_N$ (μeV)	$I^{8T}_{\max,[0\bar{1}1]}$ (nA)	$\Delta E^{8T}_{N,[0\bar{1}1]}$ (μeV)	$\langle g^*_{[0\bar{1}1],N}\rangle$	$B^N_{[\bar{2}33]}$ (T)	$\langle g^*_{[\bar{2}33],N}\rangle$
2	6.45	25	161.25	22.5	145.13	0.035		
3	4.3	27.5	118.25	22.5	96.75	0.046	3	0.56
4	3.225	50	161.25	45	145.13	0.0347	3	0.93
5	2.58	42.5	109.65	37.5	96.75	0.028	6	0.96
6	2.16	35	75.6				3.25	0.4

ment direction. Half-integer plateaus appear at the critical fields $B^{N-1/2}$, when spin splitting of the Nth level becomes equal to the disorder broadening of the level, as shown schematically in Fig. 3(d). While level broadening is different for different energy levels, we expect it to be independent of the direction of the magnetic field, and hence the ratio of g^*'s for the two orthogonal directions can be obtained from the appearance of half-integer plateaus, $B^{N-1/2}_{[1\bar{1}0]}/B^{N-1/2}_{[\bar{2}33]} = g^*_{[\bar{2}33],N}/g^*_{[1\bar{1}0],N}$. The integer plateaus disappear at the fields B^N when two neighboring levels with opposite spin intersect, and the average $\langle g^*_{[ijk],N}\rangle = (g^*_{[ijk],N} + g^*_{[ijk],N+1})/2$ can be found from $\Delta E_N = \Delta E_z = \langle g^*_{[ijk],N}\rangle \mu_B B^N_{[ijk]}$, where ΔE_N is the zero-field energy spacing of 1D subbands excluding level broadening.

Splitting and crossing of energy levels are best visualized in transconductance plots. In Figs. 3(a) and 3(b) a grayscale of dG/dV_g for the data in Figs. 1(a) and 1(b) is plotted. The white regions correspond to the plateaus; the dark regions correspond to the energy level being aligned with the Fermi energy in the leads and reflect level broadening, which is roughly half of the level spacing in our samples. At low fields the width of the plateaus decreases almost linearly with field, hence justifying the use of linear approximation, but at high fields there is a clear deviation from linear dependence. The critical fields where levels cross (B^N) and split ($B^{N-1/2}$) are indicated by triangles and circles.

Level spacing is determined from nonlinear transport spectroscopy. A logarithmic scale plot of transconductance for the same sample is shown in Fig. 3(c) with white regions representing the plateaus. By determining the maximum current $I_{\max}$ for the Nth plateau at which the transconductance is still zero, we obtain the 1D subband spacings between levels N and $N+1$ (excluding level broadening) as $\Delta E_N = eRI_{\max}$, where $R = h/2Ne^2$ is the resistance on the plateaus.

The experimental data for the channel along $[0\bar{1}1]$ are summarized in Table I(a). We obtain the energy level spacing ΔE_N for the first five energy levels using the method explained above. From the critical fields B^N we obtain the average $\langle g^*_{[ijk],N}\rangle$ for the neighboring energy levels. The ratio of the g^*s is 3 for $N = 1$ and approaches the 2D value of 1.2 for large N. The values $\langle g^*_{[0\bar{1}1]}\rangle$ do not depend on N, and we use $g^*_{[0\bar{1}1]} = 0.3$ to obtain the values for $g^*_{[\bar{2}33]}$ from the ratios $g^*_{[\bar{2}33],N}/g^*_{[1\bar{1}0],N}$. In Table I(b) we present similar data for QPCs with the channel along the $[\bar{2}33]$ direction. For these samples no half-split plateaus are observed for $B \parallel [0\bar{1}1]$ and $B^{N-1/2}$ is unattainable. We still can extract the average $\langle g^*\rangle$ values by measuring the change in the energy level spacing $\Delta E_N(0) - \Delta E_N(B) = \langle g^*\rangle \mu_B B$, as shown by bars in the schematic in Fig. 3(d). For $B \parallel [\bar{2}33]$ the introduction of g^* has questionable meaning due to anomalous behavior of half-integer plateaus and ill-defined $B^{N-1/2}$. We estimate g^* from measured B^N.

Figure 4 summarizes our results for the g^* for different confinement directions. For $B \parallel [\bar{2}33]$ spin splitting of energy levels strongly depends on the level number N for both confinement directions. For the field $B \parallel [0\bar{1}1]$, g^* is smaller and is almost independent of N. We see this trend for all the four samples we measured. We conclude that g-factor anisotropy is primarily determined by the crystalline anisotropy of spin-orbit interactions. Lateral confinement enhances the anisotropy.

So far we have ignored the diamagnetic shift of energy levels. The ratios $g^*_{[\bar{2}33],N}/g^*_{[1\bar{1}0],N}$ are not affected by this shift because they characterize the energy difference between spin states of the same orbital level. Likewise, the extracted $\langle g^*\rangle$ will not be affected by field confinement in the growth direction because the first 8–10 1D levels belong to the same lowest 2D subband. The only value to be affected by the diamagnetic shift will be $\langle g^*\rangle$ for $B \parallel I$. To estimate the correction, we approximate both vertical and lateral confinement by parabolic potentials $\hbar\omega_z = 2.4$ meV, $\hbar\omega_y = 0.3$ meV. The corrected $\langle g^*_c\rangle = \langle g^*\rangle(1 + \frac{\omega_1(B^N) - \omega_1(0)}{\omega_1(0)})$, where

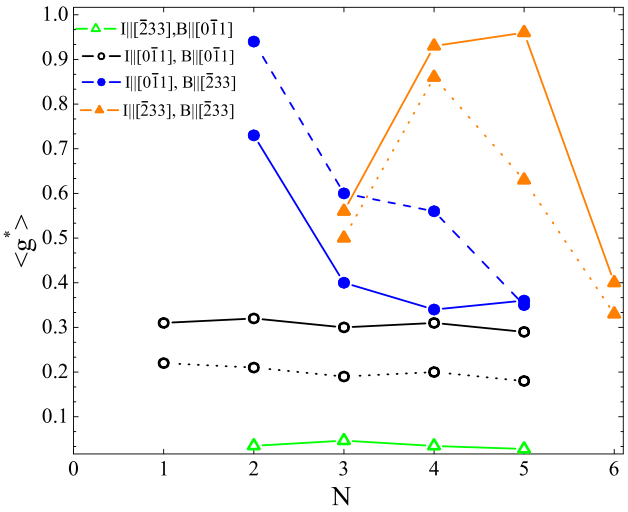

FIG. 4 (color online). (a) Average g_N^* between adjacent levels N and $N+1$ is plotted for different orientations of channel and magnetic field. Open and filled symbols are for magnetic fields parallel to $[0\bar{1}1]$ and $[\bar{2}33]$, respectively. Circles and triangles are for channels along $[0\bar{1}1]$ and $[\bar{2}33]$, respectively. The blue dashed curve is the actual g_N^* for $I \parallel [0\bar{1}1]$, $B \parallel [\bar{2}33]$. The orange and black dotted curves are corrected for the diamagnetic shift.

$\hbar\omega_1 = \frac{\hbar}{2}\sqrt{(\omega_c^2+\omega_y^2+\omega_z^2) - \sqrt{(\omega_c^2+\omega_y^2+\omega_z^2)^2 - \omega_y^2\omega_z^2}}$ is the field dependent energy spacing for spinless particles [18], $\omega_c = eB/m_c$ is the cyclotron frequency, and $m_c = \sqrt{m_h m_l} = 0.28 m_e$ is the cyclotron mass. For $I \parallel [\bar{2}33]$ the critical fields $B^N_{[\bar{2}33]} \sim 3$ T are small and the correction to $\langle g^* \rangle$ due to the diamagnetic shift is $<5\%$. For the channel along $[0\bar{1}1]$, $B^N_{[0\bar{1}1]} \sim 8$–10 T and the correction is $\sim 30\%$, which is not negligible. We plot the corrected values in Fig. 4.

Now we highlight a few qualitative differences in the appearance of "half-integer" plateaus for the channels along the $[0\bar{1}1]$ and $[\bar{2}33]$ directions. Conductance of spin-split plateaus for channels along $[0\bar{1}1]$ are quantized at $G = (N+1/2)g_0$, in full agreement with the theory. In point contacts with confinement in the orthogonal direction, conductance of spin-split plateaus is not quantized and is field dependent. At low fields ($B < 4$ T) their evolution resembles the "0.7 structure" and various anomalous plateaus reported in electron samples. At higher fields the conductance of these plateaus increases with magnetic field, at the same time the integer plateaus remain quantized at Ng_0. We emphasize the motion of spin-split plateaus with the slope of arrows in Figs. 1 and 2. For example, in Fig. 1(c) a plateau at $4.3g_0$ appears at $B \sim 3$ T, and its value gradually increases to $\sim 4.8g_0$ by 12 T. The next noninteger plateau appears at $B \sim 3$ T and increases to $\sim 6g_0$ by $B = 12$ T, while the neighboring integer plateaus remain quantized at $G = 4g_0$, $5g_0$, and $6g_0$. This feature has been observed consistently in all the samples we measured, as is evident from Fig. 2, where similar data are presented for a different sample: a plateau at $5.2g_0$ appears at $B \sim 3.3$ T and increases to $\sim 6g_0$ by 8 T. The orthogonal 1D channels are fabricated from the same 2D hole gas and have similar confinement potentials. The only difference is due to the anisotropy of spin-orbit interactions. Thus, we conclude that spin-orbit interactions are responsible for the anomalous behavior.

To summarize the results, we investigate effects of lateral confinement on spin splitting of energy levels in 2D hole gases in [311] GaAs. We found that lateral confinement enhances anisotropy of spin splitting relative to the 2D gas for both confining directions. Unexpectedly, the effective g factor does not depend on the energy level number N for $B \parallel [0\bar{1}1]$ while it has strong N dependence for the orthogonal orientation, $B \parallel [\bar{2}33]$. We also observe qualitative differences in the appearance of spin-split plateaus for the two orthogonal directions of lateral confinement, which we can attribute to the difference in spin-orbit interaction.

This work was supported by NSF Grant No. ECS-0348289.

*sunanda@purdue.edu

[1] S. A. Wolf *et al.*, Science **294**, 1488 (2001).
[2] I. Zutic, J. Fabian, and S. Das Sarma, Rev. Mod. Phys. **76**, 323 (2004).
[3] D. Loss and D. P. DiVincenzo, Phys. Rev. A **57**, 120 (1998).
[4] S. Y. Lin *et al.*, Phys. Rev. B **43**, 12110 (1991).
[5] M. Rahimi *et al.*, Phys. Rev. B **67**, 081302(R) (2003).
[6] S. J. Papadakis, E. P. De Poortere, M. Shayegan, and R. Winkler, Phys. Rev. Lett. **84**, 5592 (2000); R. Winkler, S. Papadakis, E. P. De Poortere, and M. Shayegan, *ibid.* **85**, 4574 (2000).
[7] R. Danneau *et al.*, Phys. Rev. Lett. **97**, 026403 (2006).
[8] A. J. Daneshvar *et al.*, Phys. Rev. B **55**, R13409 (1997).
[9] K. J. Thomas *et al.*, Phys. Rev. Lett. **77**, 135 (1996).
[10] A. C. Graham *et al.*, Phys. Rev. Lett. **91**, 136404 (2003).
[11] E. S. Snow and P. M. Campbell, Science **270**, 1639 (1995); R. Held *et al.*, Appl. Phys. Lett. **71**, 2689 (1997).
[12] L. P. Rokhinson, D. C. Tsui, L. N. Pfeiffer, and K. W. West, Superlattices Microstruct. **32**, 99 (2002).
[13] J. Heremans, M. Santos, K. Hirakawa, and M. Shayegan, J. Appl. Phys. **76**, 1980 (1994).
[14] D. A. Wharam *et al.*, J. Phys. C **21**, L209 (1988).
[15] B. J. van Wees *et al.*, Phys. Rev. Lett. **60**, 848 (1988).
[16] I. Zailer *et al.*, Phys. Rev. B **49**, 5101 (1994).
[17] R. Winkler, *Spin-Orbit Coupling Effects in Two-Dimensional Electron and Hole Systems,* Springer Tracts in Modern Physics Vol. 191 (Springer, Berlin, 2003).
[18] G. Salis *et al.*, Phys. Rev. B **60**, 7756 (1999).